EAI Endorsed Transactions
on Industrial Networks and Intelligent Systems
Research Article EAI.EU

A Secure Cooperative Image Super-Resolution Transmission with Decode-and-Forward Relaying over Rayleigh Fading Channels

Hien-Thuan Duong[1,3], Ca V. Phan[1,*], Quoc-Tuan Vien[2]

[1]Faculty of Electrical and Electronics Engineering, Ho Chi Minh City University of Technology and Education, Ho Chi Minh City 70000, Vietnam

[2]Faculty of Science and Technology, Middlesex University, London NW4 4BT, UK

[3]Faculty of Electronics and Telecommunications, Saigon University, Ho Chi Minh City 70000, Vietnam

Abstract

In addition to susceptibility to performance degradation due to hardware malfunctions and environmental influences, wireless image transmission poses risks of information exposure to eavesdroppers. This paper delves into the image communications within wireless relay networks (WRNs) and proposes a secure cooperative relaying (SCR) protocol over Rayleigh fading channels. In this protocol, a source node (referred to as Alice) transmits superior-resolution (SR) images to a destination node (referred to as Bob) with the assistance of a mediating node (referred to as Relay) operating in decode-and-forward mode, all while contending with the presence of an eavesdropper (referred to as Eve). In order to conserve transmission bandwidth, Alice firstly reduces the size of the original SR images before transmitting them to Relay and Bob. Subsequently, random linear network coding (RLNC) is employed by both Alice and Relay on the down-scaled poor-resolution (PR) images to obscure the original images from Eve, thereby bolstering the security of the image communications. Simulation results demonstrate that the proposed SCR protocol surpasses both secure relaying transmission without a direct link and secure direct transmission without relaying links. Additionally, a slight reduction in image quality can be achieved by increasing the scaling factor for saving transmission bandwidth. Furthermore, the results highlight the SCR protocol's superior effectiveness at Bob's end when compared to Eve's, which is due to Eve's lack of access to the RLNC coefficient matrices and reference images utilised by Alice and Relay in the RLNC process. Finally, the evaluation of reference images, relay allocations and diversity reception over Rayleigh fading channels confirms the effectiveness of the SCR protocol for secure image communications in the WRNs.

Keywords: Image communication; Deep learning; Image super-resolution; Random linear network coding; Cooperative communications; Wireless relay networks

Received on 21 March 2024, accepted on 02 August 2024, published on 02 September 2024

doi: 10.4108/eetinis.v11i4.6193

1. Introduction

The increasing fascination with collaborative wireless communication stems from innovative advancements that enhance the security and dependability of data transmission. The intermediary participants, known as relay nodes, facilitate a cooperative link between two terminal users through the shared wireless media [1]. Such cooperative strategies have been integrated into various wireless network structures in which the deployment of the relay nodes not only amplifies the overall system capacity and extends the network's coverage but also concurrently elevates signal fidelity and augments the benefits derived from spatial diversity [2].

Relay nodes in wireless relay networks (WRNs) possess the capability to process and store data, acting both before it is dispatched to the destination nodes and after reception from the source nodes. The throughput of the WRNs has seen a significant enhancement with the adoption of the network coding (NC) concept, first introduced in [3]. This technique, when applied at the relay nodes, serves to bolster the data transmission rate of the wireless relay network, as evidenced by [4, 5]. In

*Corresponding author. Email: capv@hcmute.edu.vn

NC, a relay node or a source applies a coding function to numerous packets it receives from input to form a output packet. The coding function might be linear or nonlinear, deterministic or probabilistic, depending on the specific applications. For instance, in random linear network coding (RLNC) [6], nodes integrate input packets linearly using randomly selected coefficients to construct the coding function. Provided that a sufficient quantity of mixed data packets is available, and the destination nodes possess knowledge of the linear coefficients, they have the ability to retrieve the original data from the source nodes [7]. A variety of protocols rooted in NC have been devised for prevalent relay channel frameworks. These include protocols for relay-supported bilateral channels [8], broadcasting channels [9], and multi-channels [10]. Additionally, RLNC enhances security by limiting the degrees of freedom (essentially the decoding potential) that an eavesdropper can exploit, thereby protecting the communications [11].

In the context of image transmission over wireless relay networks (WRNs), image data from a source node can be delivered to a destination node either directly or through a dual-hop process with the support of a relay node (for instance, via source-to-relay and relay-to-destination links). Motivated by the advantageous impact of cooperative diversity, this study delves into a collaborative communication approach aimed at boosting the efficacy of image transfers in WRNs by leveraging both relay and direct connections. Although image transmission can be executed using RLNC and standard relaying methods, it is crucial to consider various challenges related to data privacy and the bandwidth required for transmission. This research introduces a secure collaborative communication protocol that minimizes the bandwidth demands for image transfers in WRNs and concurrently conceals the image content. This is achieved by drawing on the principles of RLNC and image super-resolution (ISR). The principal contributions of this research are outlined as follows:

- The study broadens the assessment of the secure image communication model's efficacy, as proposed in [12], within a fading radio environment. It introduces a secure collaborative wireless communication method for transmitting images between Alice and Bob in WRNs, with the aid of a relay user. To conserve bandwidth, Alice's original superior-resolution (SR) image is initially down-scaled using the suggested technique. This reduced poor-resolution (PR) image is then merged with a reference image through RLNC encoding, which effectively masks the true image from Eve, a potential eavesdropper. Following RLNC encoding, the composite image is binary-converted and processed for transmission across the fading channel using channel coding and digital modulation. At the relay and Bob's end, the reverse process is executed, involving signal equalization, demodulation, and channel decoding. Bob can then apply RLNC decoding and ISR to reconstruct Alice's original SR image from the relayed data. The proposed method's intrigue lies in its efficient fusion of RLNC and ISR benefits into a unified protocol for image communication in WRNs, particularly when operating under constrained bandwidth. Notably, in scenarios with high signal-to-noise ratio (SNR), there exists a delicate balance between bandwidth conservation and the quality of the restored SR image.

- The placement of the relay node significantly influences the performance of the proposed protocol. The intersection of Source-Relay Transmission (SRT) and Source-Destination Transmission (SDT) delineates two operational zones: low-SNR and high-SNR. In the low-SNR region, SRT outperforms SDT, while the reverse is true in the high-SNR domain. Overall, the Secure Cooperative Relay (SCR) protocol surpasses both SRT and SDT across the entire evaluation spectrum. Notably, the SCR protocol exhibits marginally superior performance when the relay is positioned closer to the destination (near Bob) compared to when it is situated near the source (near Alice).

- The research reveals that the format, dimensions, attributes, and structural discrepancies of the reference images distinctly impact the SCR protocol's efficiency. Conversely, the effectiveness of Eve's decoding attempts fluctuates with the use of various inaccurately estimated images; nevertheless, the performance remains substantially subpar, and the recovery of Alice's original superior-resolution (SR) image is unattainable.

- The proposed SCR protocol falls under the category of Decode and Forward (DF) cooperative protocols. Consequently, diversity reception techniques such as Maximal Ratio Combining (MRC), Equal Gain Combining (EGC), and Selection Combining (SC) can be utilized to improve performance. This is particularly effective when the relay has access to the identical shared reference image and RLNC coefficient matrix as Alice.

The structure of the remaining sections of the article is as follows: Section 2 introduces the pertinent literature that lays the groundwork and serves as the impetus for our investigation. Section 3 delineates the system architecture for conventional image communication

within a WRN that includes wiretap links. The proposed SCR protocol, designed for safeguarded ISR across WRNs, is detailed in Section 4. Section 5 is dedicated to showcasing simulation outcomes that substantiate the SCR protocol's efficacy and benchmark it against alternative protocols. The article reaches its culmination in Section 6, summarizing the key findings and proposing avenues for future exploration.

2. Related Works

Graphic language is a ubiquitous element in our daily lives, and ensuring the integrity and confidentiality of superior-resolution image transmission over a lossy, bandwidth-constrained wireless channel remains a significant scientific challenge. Historically, the approach in [13] involved a combined source and channel coding technique for transmitting images over block erasure channels, where higher frequencies receive minimal shielding and lower frequencies are more robustly protected by channel codes. The synergy of channel coding and source coding is also explored in [14]. Furthermore, the work in [15] proposes an optimization framework that devises an authentication graph, which strategically allocates additional redundant authentication data to the most critical image packets.

In the realm of image processing, the technique known as Image Super-Resolution (ISR) has garnered significant interest in recent times. This process involves generating superior-resolution images from poor-resolution counterparts. The rapid advancements in deep learning have propelled deep learning-based ISR methods to surpass traditional approaches, as documented in references [16–18]. This progress has given rise to various ISR frameworks, such as the super-resolution feedback network [19], deep residual network [20], super-resolution convolutional neural network [21], Laplacian pyramid SR [22], deep back-projection networks [23], and the VDSR (Very Deep Super Resolution) [24]. An aggregate based on deep learning (DL), such as the Reliability-Aware Neural Network (RANN) [25], has been employed to enhance performance in signature categorization tasks. The VDSR, in particular, has demonstrated its capability to reconstruct superior-resolution images from poor-resolution versions, delivering impressive performance and operational speed. Within the VDSR architecture, each convolutional layer is equipped with 64 filters and rectified linear units. Thanks to its robust design, VDSR has been applied across diverse fields, including image communications [26], industrial machinery [27], seismic analysis [28], and network security [29]. It's important to highlight that the use of lower-resolution images plays a pivotal role in reducing the bandwidth required for transmission.

Considering privacy in the realm of image communication is essential. Picture protection can be broadly divided into two techniques: cryptography and information concealment. The latter includes watermarking and steganography as its subcategories. Cryptography employs encryption or hashing to scramble an image, which is then decrypted at the receiver's end to reveal the hidden image. A particular strategy using secure image hash-based geometric alterations was proposed in reference [30] to safeguard images with minimal shared details. Employing transformations such as rotation, shift, and scale can enhance image security. Reference [31] explores various encryption methods. Watermarking involves embedding digital data within a host image, which can serve to authenticate images or protect copyrights and may be either visible or invisible. Reference [32] discusses an advanced method combining semi-tensor product and compressed sensing for digital watermarking, aimed at securing telemedicine image transmissions. This technique has proven highly effective against various disturbances, including white Gaussian noise, Poisson noise, and impulsive noise. Additionally, steganography is a popular method for concealing information within other non-sensitive data, as mentioned in references [33] and [34]. Although their techniques vary, both aim to keep the data protected from unauthorized access. Steganography is often favored over encryption due to its simplicity, as it does not require complex encryption and decryption algorithms at both ends. It is a versatile technique that can conceal text, images, audio, and video; however, images with ample redundant bits are particularly well-suited for this purpose. A straightforward method involving the least significant bit was introduced in [35], utilizing the final bit of each pixel to store the secret message's data bits. The concealment can be further enhanced through the use of DWT (Discrete Wavelet Transform) [36] and DCT (Discrete Cosine Transform) [37], which transition the image from the spatial to the frequency domain, allowing alterations across various frequency bands without detection. The application of this technique may be constrained by the requirement that the hidden image be smaller than the cover image. In contrast to traditional image steganography, coverless steganography embeds secret data directly into the cover image's edge, texture, brightness, and color, without any overt alterations or markings. This innovative approach has seen significant contributions, as documented in [38]. For evaluating the performance of secure image transmission, various metrics have been listed in [39], including MSE (Mean Square Error), MAE (Mean Absolute Error), PSNR (Peak Signal-to-Noise Ratio), Image Entropy, Throughput, NPCR (Number of Pixel Change Rate), CC (Correlation Coefficient), NC (Normalized Coefficient), Hiding Capacity, and SSIM (Structural Similarity Index). Among these,

PSNR and SSIM [40] are well-known and frequently used for assessment. Detailed explanations of PSNR and SSIM will be provided in Section 5.

The NC has been widely adopted in scholarly works to enhance the throughput of information transmission over WRNs, as referenced in [41, 42]. The inception of a secure NC methodology was introduced in [43]. Research detailed in [11] demonstrated that RLNC can protect communications within a network susceptible to interception by intermediate nodes. Implementing NC at the physical layer of a two-way relay wireless network has been shown to potentially double system throughput, a concept initially put forth in [41]. Secure relaying strategies, such as the modify-and-forward approach in WRNs where the relay fuses decoded data with an encrypted key in a random linear fashion before relaying to the destination, have been employed as per [44] to fortify the security against wiretap channels. The authors in [45] advocate for the use of RLNC and relay selection techniques to bolster security, reduce latency, and cut down on energy consumption in WRNs. Hybrid NC, outlined in [46], is presented as a strategy to enhance the security of wireless channels. This approach involves splitting the NC output into two segments: one is openly broadcasted, while the other is secured through covert security measures at the physical layer.

Based on these techniques, we have created a secure collaborative relaying protocol across WRNs. To secure images communicated within the network, we achieve this by combining the RLNC concept with a reference image that acts as coverless steganography. Furthermore, in order to preserve transmission bandwidth at Bob and the relay, we use ISR to retrieve the original SR photos from their PR versions.

3. System Model

In our study, we employed a standard four-node system model depicted in Fig.1 to assess the security of image communication over fading WRN. The model consists of a sender, Alice ($\mathcal{A}$), who aims to transmit a confidential image to the recipient, Bob ($\mathcal{B}$), either directly or via a relay node, Relay ($\mathcal{R}$). An eavesdropper, Eve ($\mathcal{E}$), is positioned to intercept the image during its transmission from Alice or through Relay. As illustrated in Fig.1, two potential wiretap links are highlighted in red. The model takes into account the spatial positioning of the nodes, denoted by coordinates $(x_{\mathcal{A}}, y_{\mathcal{A}})$ for $\mathcal{A}$ (Alice), $(x_{\mathcal{R}}, y_{\mathcal{R}})$ for $\mathcal{R}$ (Relay), $(x_{\mathcal{B}}, y_{\mathcal{B}})$ for $\mathcal{B}$ (Bob) and $(x_{\mathcal{E}}, y_{\mathcal{E}})$ for $\mathcal{E}$ (Eve). Transmission of images between between nodes $\mathcal{S}$ and $\mathcal{D}$, where $\mathcal{S} \in \{\mathcal{A}, \mathcal{R}\}$, and $\mathcal{D} \in \{\mathcal{R}, \mathcal{B}, \mathcal{E}\}$, is subject to the effects of a wireless fading channel, which in our assumption is a flat Rayleigh fading channel, and the additive white Gaussian noise (AWGN) at the receiver's end. The physical distances between these nodes are also factored into the system model.

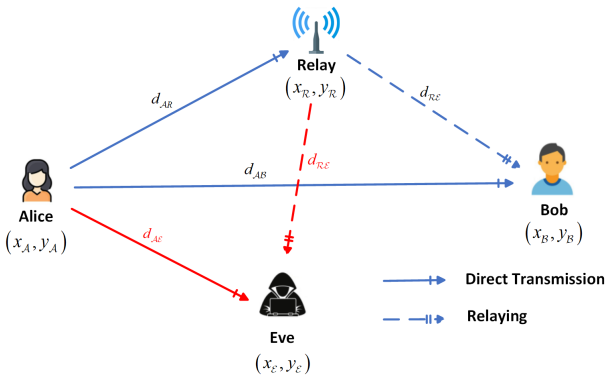

Figure 1. System model of secure image communications in a typical WRN.

In this study, we concentrate on a color image, denoted as $\mathbf{W}$, with dimensions $P \times Q$, represented by a three-dimensional array of size $P \times Q \times 3$. It is expected that the communication of channels and decoding information between Bob, Alice, and Relay will be seamless over the assumed channels. The proposed SCR protocol enables image transmission between Alice and Bob in two distinct phases: (i) In the first phase, Alice sends the RLNC-encoded image to both Bob and Relay; (ii) In the subsequent phase, Relay decodes the received image, re-encrypts it using RLNC and forwards the newly encoded image to Bob. Throughout both phases, Eve has the potential to intercept the communication over the shared wireless network and may attempt to decipher the images transmitted by Alice and Relay using the wiretap links.

4. Secure Collaborative Relaying for Image Communications

The protocol examined in this study mirrors the one detailed in reference [12]. Our investigation extends to analyzing the positions of the network nodes and the impact of the wireless fading channel on the SCR protocol. A comprehensive depiction of the protocol can be found in Fig.2.

4.1. Signal Processing at Alice

Alice first uses bicubic interpolation (this work considers the bicubic filter because of its low processing complexity) to downscale the original SR image into an PR version in order to minimize the amount of transmission bandwidth required.

Alice is given an original RGB image, denoted as $\mathbf{W}_{\mathcal{A}}^{(SR)}$, with dimensions $P \times Q \times 3$. This image is intended to be transmitted to Bob. To create a

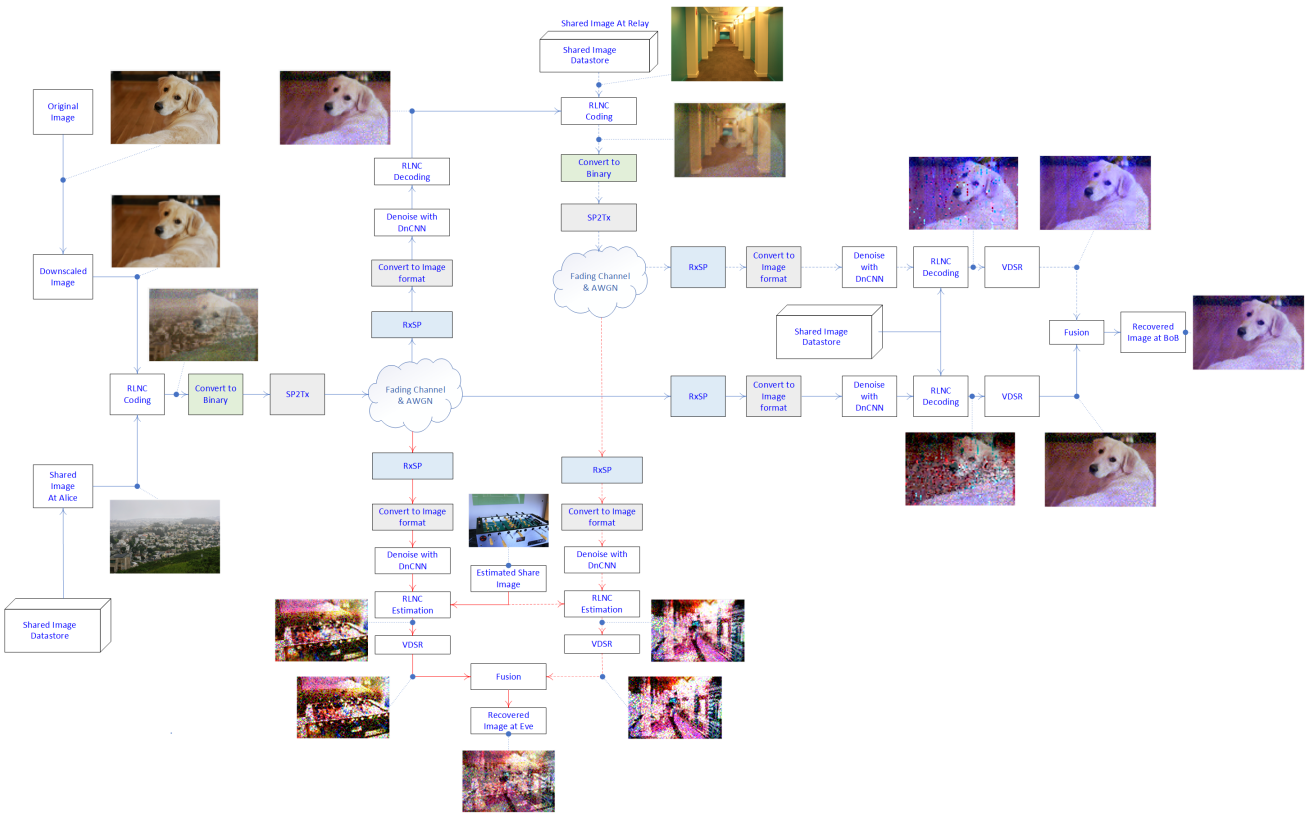

Figure 2. Proposed SCR for image communications with ISR.

poor resolution (PR) version of this image, bicubic interpolation is applied using a scaling factor τ, resulting in $\mathbf{W}_{\mathcal{A}}^{(PR)}$ with new dimensions $P' \times Q' \times 3$. Here, P' is the smallest integer greater than or equal to $P' = \lceil P/\tau \rceil$ and Q' is the smallest integer greater than or equal to $Q' = \lceil Q/\tau \rceil$, indicated by the ceiling function $\lceil \cdot \rceil$. For security reasons, RLNC is employed to encode $\mathbf{W}_{\mathcal{A}}^{(PR)}$. This process involves blending the PR image with a reference image, $\mathbf{W}_{\mathcal{A}}^{(ref)}$, which is randomly selected from a shared image datastore, $\mathfrak{S}$. The resulting encoded image at Alice's end is referred to as $W_{\mathcal{A}}^{(enc)}$.

$$\mathbf{W}_{\mathcal{A}}^{(enc)} = \mathbf{N}_{\mathcal{A},1} \otimes \mathbf{W}_{\mathcal{A}}^{(PR)} + \mathbf{N}_{\mathcal{A},2} \otimes \mathbf{W}_{\mathcal{A}}^{(ref)} \tag{1}$$

In the context provided, $\mathbf{N}_{\mathcal{A},i}$, $i \in \{1, 2\}$,, refers to RLNC coefficient matrices at Alice, each with dimensions $P' \times Q' \times 3$. The symbol, $\otimes$, represents the element-wise multiplication, also known as the Hadamard product, between two matrices. For any given element in the matrix $\mathbf{N}_{\mathcal{A},i}$, represented as $\gamma_{\mathcal{A},p,q,k}^{(i)}$, where $p \in \{1, 2, \ldots, P'\}$, $q \in \{1, 2, \ldots, Q'\}$, $k \in \{1, 2, 3\}$, it signifies the coefficient at the corresponding position in the matrix. To ensure that the pixel values of the encoded image remain within the acceptable range, each coefficient $\gamma_{\mathcal{A},p,q,k}^{(i)}$ is constrained to be within the interval $[0, 1]$. Additionally, for every position (p, q, k), the sum of the coefficients from both matrices must equal 1, expressed as $\gamma_{\mathcal{A},p,q,k}^{(1)} + \gamma_{\mathcal{A},p,q,k}^{(2)} = 1$. [1] The RLNC-encoded image, $\mathbf{W}_{\mathcal{A}}^{(enc)}$, undergoes a binary conversion and is then processed through SP2Tx (Signal Processing to Transmit), which involves channel coding and modulation. This coding method introduces redundancy into the binary data to enhance the reliability of communication. Specifically, this paper utilizes a straightforward 1/2 convolutional coding scheme with a constraint length of $K_{cons} = 3$ and a generator polynomial of $[111, 101]$. For the transmission of the binary data over a wireless communication channel, digital modulation is necessary. This process involves the correspondence between the binary data and signal sequences based on the chosen modulation technique. In this case, a simple Binary Phase Shift Keying (BPSK) modulation is employed. The output from SP2Tx, denoted as $x_{\mathcal{A}}$, is sent to Bob. However, during the initial transmission slot, the Relay is susceptible to eavesdropping by Eve. It is assumed that the distance between the source ($\mathcal{S}$)

[1] *Effects of coefficient matrices for RLNCs,* $\gamma_{\mathcal{A},p,q,k}^{(i)}$, and *Impact of scale factor,* τ, are mentioned in [12]

and destination ($\mathcal{D}$) is $d_{\mathcal{SD}}$, where $\mathcal{S} \in \{\mathcal{A}, \mathcal{R}\}$ and $\mathcal{D} \in \{\mathcal{R}, \mathcal{D}, \mathcal{E}\}$.

4.2. Signal Processing at Relay

In the initial time slot, the signal that the Relay receives can be represented as follows:

$$y_{\mathcal{R}}^{(1)} = \frac{h_{\mathcal{AR}} x_{\mathcal{A}}}{d_{\mathcal{AR}}^{\beta}} + g_{\mathcal{R}}^{(1)} \tag{2}$$

In the given context, $h_{\mathcal{AR}}$ represents the fading channel gain, and $d_{\mathcal{AR}}^{\beta}$ denotes the path loss from $\mathcal{A}$ to $\mathcal{R}$, with β being the path loss factor. The term $g_{\mathcal{R}}^{(1)}$ refers to an independent Additive White Gaussian Noise (AWGN) at the $\mathcal{R}$ node, characterized by a zero mean and a variance of $\sigma_{\mathcal{R},1}^2$ for each element. The channel is assumed to be flat fading, which means it has only a single tap in the multipath channel, simplifying the convolution to a mere multiplication. The received signal undergoes processing in RxSP (Received Signal Processing), where it is equalized, demodulated, and channel-decoded using the Viterbi algorithm for maximum likelihood estimation. After processing, the signal is converted back into an image format, resulting in the estimated image, denoted as $\hat{\mathbf{X}}_{\mathcal{R}}^{(1)}$. To remove noise from the image, a pretrained deep neural network known as DnCNN [28] is employed, producing the denoised image at $\mathcal{R}$, represented as $\bar{\mathbf{W}}_{\mathcal{R}}^{(1)}$. Utilizing the shared reference image from $\mathcal{A}$, $\mathbf{W}_{\mathcal{A}}^{(ref)}$, along with the RLNC coefficient matrices, $\mathbf{N}_{\mathcal{A},1}$ and $\mathbf{N}_{\mathcal{A},2}$, the $\mathcal{R}$ is able to estimate the original poor-resolution image, $\mathbf{W}_{\mathcal{A}}^{(PR)}$, as

$$\hat{\mathbf{W}}_{\mathcal{R}}^{(1)} = \left(\bar{\mathbf{W}}_{\mathcal{R}}^{(1)} - \mathbf{N}_{\mathcal{A},2} \otimes \mathbf{W}_{\mathcal{A}}^{(ref)}\right) \oslash \mathbf{N}_{\mathcal{A},1}, \tag{3}$$

In the context provided, the symbol, $\oslash$, is used to indicate the element-wise division between two matrices. This means that each element in one matrix is divided by the corresponding element in the other matrix.

During the second time slot, the estimated image at the Relay, denoted as $\hat{\mathbf{W}}_{\mathcal{R}}^{(1)}$, is combined with a reference image, $\mathbf{W}_{\mathcal{R}}^{(ref)}$. This reference image at the Relay may or may not be identical to the one at Alice's end, but it is also randomly chosen from the same shared image datastore, $\mathfrak{S}$, accessible to all authorized users. The RLNC-encoded image at the Relay is expressed as:

$$\mathbf{W}_{\mathcal{R}}^{(enc)} = \mathbf{N}_{\mathcal{R},1} \circ \hat{\mathbf{W}}_{\mathcal{R}}^{(1)} + \mathbf{N}_{\mathcal{R},2} \circ \mathbf{W}_{\mathcal{R}}^{(ref)}, \tag{4}$$

Here, $\mathbf{N}_{\mathcal{R},i}$, $i \in \{1, 2\}$, are RLNC coefficient matrices at the Relay, each with dimensions $P' \times Q' \times 3$. The coefficient in matrix $\mathbf{N}_{\mathcal{R},i}$ at position (p, q, k) is represented by $\gamma_{\mathcal{R},p,q,k}^{(i)}$, $p \in \{1, 2, \ldots, P'\}$, $q \in \{1, 2, \ldots, Q'\}$, $k \in \{1, 2, 3\}$. These coefficients are constrained to ensure that the pixel values of the encoded image at the Relay do not exceed their permissible range, meaning $0 \leq \gamma_{\mathcal{R},p,q,k}^{(i)} \leq 1$ and the sum of the coefficients for each position equals one, $\gamma_{\mathcal{R},p,q,k}^{(1)} + \gamma_{\mathcal{R},p,q,k}^{(2)} = 1$. The RLNC-encoded image, $\mathbf{W}_{\mathcal{R}}^{(enc)}$, undergoes the same processing as at Alice's end before being transmitted over the fading channel. This includes conversion to binary, channel encoding, and modulation. The processed signal is then conveyed to Bob as a wireless signal, symbolized by $x_{\mathcal{R}}$.

4.3. Signal Processing at Bob

In the initial time slot, the signal that Bob receives from Alice is expressed as:

$$y_{\mathcal{B}}^{(1)} = \frac{h_{\mathcal{AB}} x_{\mathcal{A}}}{d_{\mathcal{AB}}^{\beta}} + g_{\mathcal{B}}^{(1)} \tag{5}$$

Here, $h_{\mathcal{AB}}$ and $d_{\mathcal{AB}}^{\beta}$ represent the fading channel gain and path loss from Alice to Bob, respectively, with β being the path loss factor. The term $g_{\mathcal{B}}^{(1)}$ is an independent AWGN at Bob's node, characterized by a zero mean and a variance of $\sigma_{\mathcal{B},1}^2$ for each symbol, which is assumed to be equal to $\sigma_{\mathcal{R},1}^2$. Similar to the process at the Relay, the signal received by Bob is processed through RxSP, where it is equalized, demodulated, and channel-decoded using the Viterbi algorithm. Passing RxSP, the signal is transformed into an image format, resulting in the estimated signal, $\hat{\mathbf{X}}_{\mathcal{B}}^{(1)}$. This image is then denoised using a DnCNN network [28]. The denoised and estimated original poor-resolution image at Bob is denoted as $\hat{\mathbf{W}}_{\mathcal{B}}^{(1)}$.

$$\hat{\mathbf{W}}_{\mathcal{B}}^{(1)} = \left(\bar{\mathbf{W}}_{\mathcal{B}}^{(1)} - \mathbf{N}_{\mathcal{A},2} \otimes \mathbf{W}_{\mathcal{A}}^{(ref)}\right) \oslash \mathbf{N}_{\mathcal{A},1}, \tag{6}$$

where $\bar{\mathbf{W}}_{\mathcal{B}}^{(1)}$ is an estimated image after denoising. $\mathbf{N}_{\mathcal{A},1}$ and $\mathbf{N}_{\mathcal{A},2}$ are RLNC coefficient matrices used at Alice. Following RLNC-decoding, Bob reconstructs the full-size original superior-resolution (SR) image using an VDSR ISR framework [24]. This VDSR ISR framework was trained on the publicly available IAPR TC-12 Benchmark dataset [47]. The training hyper-parameters for the proposed SCR protocol were set to a batch size of 64 across 100 epochs, with an initial learning rate of 0.1 and various scaling factors $\tau = \{2, 4, 6, 8, 10\}$. Consequently, the SR image that Bob recovers in the first time slot, denoted as $\hat{\mathbf{W}}_{\mathcal{B}}^{(SR,1)}$, is acquired through this method.

$$\hat{\mathbf{W}}_{\mathcal{B}}^{(SR,1)} = \Delta_{\tau}(\hat{\mathbf{W}}_{\mathcal{B}}^{(1)}), \tag{7}$$

In the given context, the symbol $\Delta_{\tau}(\cdot)$ represents the VDSR ISR operator used to reconstruct superior-resolution (SR) images. The scaling factor, denoted by τ,

is a parameter that determines the degree of upscaling applied to enhance the image resolution.

In the second time slot, Bob receives a signal from the Relay, which is formulated as:

$$y_{\mathcal{B}}^{(2)} = \frac{h_{\mathcal{RB}} x_{\mathcal{R}}}{d_{\mathcal{RB}}^{\beta}} + g_{\mathcal{B}}^{(2)} \tag{8}$$

where $h_{\mathcal{RB}}$ and $d_{\mathcal{RB}}^{\beta}$ are the fading channel gain and path loss from the Relay to Bob, respectively; β is the path loss exponent, and $g_{\mathcal{B}}^{(2)}$ is an independent AWGN at Bob's node with zero mean and a variance of $\sigma_{\mathcal{B},2}^2$ for each symbol.

If the reference image at the Relay is different from Alice's, Bob's signal processing in the second time slot mirrors that of the first time slot when he received the signal from Alice. The received signal from the Relay is processed through RxSP and then converted into an image format, yielding the estimated image $\hat{\mathbf{X}}_{\mathcal{B}}^{(2)}$.

Alternatively, if the Relay and Alice use the same reference image, the received signal at Bob in the second time slot can benefit from diversity receiving techniques such as Maximum Ratio Combining (MRC), Equal Gain Combining (EGC), and Selection Combining (SC). The equalization process for combining the signals from the two time slots is outlined in the communication protocol as

$$\hat{y}_{\mathcal{B}.\mathcal{MRC}}^{(2)} = h_{\mathcal{AB}}^{*} y_{\mathcal{B}}^{(1)} + h_{\mathcal{RB}}^{*} y_{\mathcal{B}}^{(2)} \tag{9}$$

$$\hat{y}_{\mathcal{B}.\mathcal{EGC}}^{(2)} = e^{-j\angle h_{\mathcal{AB}}} y_{\mathcal{B}}^{(1)} + e^{-j\angle h_{\mathcal{RB}}} y_{\mathcal{B}}^{(2)} \tag{10}$$

$$\hat{y}_{\mathcal{B}}^{(2)} = \begin{cases} h_{\mathcal{AB}}^{-1} y_{\mathcal{B}}^{(1)} & if\ \gamma_{\mathcal{B}}^{(1)} > \gamma_{\mathcal{B}}^{(2)} \\ h_{\mathcal{RB}}^{-1} y_{\mathcal{B}}^{(2)} & if\ \gamma_{\mathcal{B}}^{(2)} > \gamma_{\mathcal{B}}^{(1)} \end{cases} \tag{11}$$

where $y_{\mathcal{B}}^{(1)}$ and $y_{\mathcal{B}}^{(2)}$ are in Eq.(5) and Eq.(8), respectively; $\gamma_{\mathcal{B}}^{(1)}$ and $\gamma_{\mathcal{B}}^{(2)}$ are the instantaneous SNRs associated with the $\mathcal{A}-\mathcal{B}$ and $\mathcal{R}-\mathcal{B}$ channels. Those equalized signals will be demodulated and channel decoded (with Viterbi Algorithm) then converted to image format. Then we have the estimated image, $\hat{x}_{\mathcal{B}.\mathcal{DR}}^{(2)}$ where $\mathcal{DR} \in \{\mathcal{MRC}, \mathcal{EGC}, \mathcal{SC}\}$. The estimated image $\hat{\mathbf{X}}_{\mathcal{B}}^{(2)}$ or $\hat{\mathbf{X}}_{\mathcal{B}.\mathcal{DR}}^{(2)}$ is denoised by using DnCNN network to get denoised PR image $\bar{\mathbf{W}}_{\mathcal{B}}^{(2)}$ or $\bar{\mathbf{W}}_{\mathcal{B}.\mathcal{DR}}^{(2)}$. Bob can use RLNC decoding to retrieve the PR image that was sent from Relay in the manner described below.

$$\hat{\mathbf{W}}_{\mathcal{B}}^{(2)} = \left(\bar{\mathbf{W}}_{\mathcal{B}}^{(2)} - \mathbf{N}_{\mathcal{R},2} \otimes \mathbf{W}_{\mathcal{R}}^{(ref)}\right) \oslash \mathbf{N}_{\mathcal{R},1}. \tag{12}$$

$$\hat{\mathbf{W}}_{\mathcal{B}.\mathcal{DR}}^{(2)} = \left(\bar{\mathbf{W}}_{\mathcal{B}.\mathcal{DR}}^{(2)} - \mathbf{N}_{\mathcal{A},2} \otimes \mathbf{W}_{\mathcal{A}}^{(ref)}\right) \oslash \mathbf{N}_{\mathcal{A},1}. \tag{13}$$

To recover the image transferred from Relay, keep in mind that Bob needs access to both the reference image and the RLNC coefficient matrices used for RLNC encoding at the Relay. Bob converts PR received image to SR orignal image by employing an VDSR ISR framework which is presented by $\hat{\mathbf{W}}_{\mathcal{B}}^{(SR,2)}$ or $\hat{\mathbf{W}}_{\mathcal{B}.\mathcal{DR}}^{(SR,2)}$

$$\hat{\mathbf{W}}_{\mathcal{B}}^{(SR,2)} = \Delta_{\tau}(\hat{\mathbf{W}}_{\mathcal{B}}^{(2)}). \tag{14}$$

$$\hat{\mathbf{W}}_{\mathcal{B}.\mathcal{DR}}^{(SR,2)} = \Delta_{\tau}(\hat{\mathbf{W}}_{\mathcal{B}.\mathcal{DR}}^{(2)}). \tag{15}$$

Ultimately, Bob creates a composite image by layering the superior-resolution images recovered from both time slots. The process involves superimposing $\hat{\mathbf{W}}_{\mathcal{B}}^{(SR,1)}$ from Eq.(7) and $\hat{\mathbf{W}}_{\mathcal{B}}^{(SR,2)}$ from Eq.(14), or $\hat{\mathbf{W}}_{\mathcal{B}.\mathcal{DR}}^{(SR,2)}$ from Eq.(15), resulting in:

$$\hat{\mathbf{W}}_{\mathcal{B}}^{(SR)} = \alpha_1 \hat{\mathbf{W}}_{\mathcal{B}}^{(SR,1)} + \alpha_2 \hat{\mathbf{W}}_{\mathcal{B}}^{(SR,2)}, \tag{16}$$

$$\hat{\mathbf{W}}_{\mathcal{B}.\mathcal{DR}}^{(SR)} = \alpha_1 \hat{\mathbf{W}}_{\mathcal{B}}^{(SR,1)} + \alpha_2 \hat{\mathbf{W}}_{\mathcal{B}.\mathcal{DR}}^{(SR,2)}, \tag{17}$$

Here, α_i, where $i \in 1, 2$, indicates the proportion of the i-th superior-resolution image that contributes to the final blended image. α_i is also called Alpha blending factor [48] in image fusion techniques.

4.4. Signal Processing at Eve

Due to the broadcast characteristics of the wireless medium, Eve may intercept the data packets transmitted by Alice and the Relay during both time slots, even though they are not intended for her. The formulas representing the signals that Eve captures in the first and second time slots can be articulated accordingly. This highlights the potential security concerns in wireless communication where unintended recipients can access the transmitted data.

$$y_{\mathcal{E}}^{(1)} = \frac{h_{\mathcal{AE}} x_{\mathcal{A}}}{d_{\mathcal{AE}}^{\beta}} + g_{\mathcal{E}}^{(1)} \tag{18}$$

$$y_{\mathcal{E}}^{(2)} = \frac{h_{\mathcal{RE}} x_{\mathcal{R}}}{d_{\mathcal{RE}}^{\beta}} + g_{\mathcal{E}}^{(2)} \tag{19}$$

where $h_{\mathcal{ZE}}$, $d_{\mathcal{ZE}}^{\beta}$ are fading channel gain and path loss from $\mathcal{Z}$ (with $\mathcal{Z} \in \{\mathcal{A}, \mathcal{R}\}$) to $\mathcal{E}$, respectively; β is path loss factor; $g_{\mathcal{E}}^{(i)}$, $i \in \{1, 2\}$, is an AWGN at Eve in the i-th time slot with each entry having zero mean and variance of $\sigma_{\mathcal{E},i}^2$. Eve attempts to discern the origin of the data—whether it's from Alice or the Relay—using the same methods as the Relay and Bob. The signals received are processed through RxSP, where they are equalized, demodulated, and channel-decoded. The output from RxSP yields the estimated signals for both time slots, denoted as $\hat{\mathbf{X}}_{\mathcal{E}}^{(1)}$ and $\hat{\mathbf{X}}_{\mathcal{E}}^{(2)}$. These estimated signals are then converted into image format and subsequently denoised using a deep neural network equipped with a pretrained DnCNN network,

resulting in the denoised images $\bar{\mathbf{W}}_{\mathcal{E}}^{(1)}$ and $\bar{\mathbf{W}}_{\mathcal{E}}^{(2)}$. Eve is unaware of the RLNC coefficient matrices, denoted as $\{\mathbf{N}_{\mathcal{A},1}, \mathbf{N}_{\mathcal{A},2}\}$ and $\{\mathbf{N}_{\mathcal{R},1}, \mathbf{N}_{\mathcal{R},2}\}$ which Alice and Relay utilize to conceal the original image. She also lacks knowledge of the reference images, $\mathbf{W}_{\mathcal{A}}^{(ref)}$ and $\mathbf{W}_{\mathcal{R}}^{(ref)}$, stored in the image database and accessible only to authorized individuals. Eve attempts to deduce the RLNC coefficient matrices and searches the database for the reference images to recover the original images. The approximated RLNC coefficient matrices at Alice and Relay are represented by $\{\hat{\mathbf{N}}_{\mathcal{A},1}, \hat{\mathbf{N}}_{\mathcal{A},2}\}$ and $\{\hat{\mathbf{N}}_{\mathcal{R},1}, \hat{\mathbf{N}}_{\mathcal{R},2}\}$. The elements of the RLNC coefficient matrices at Alice and Relay can be estimated using the following method:

$$\hat{\gamma}_{\mathcal{X},p,q,k}^{(1)} = \gamma_{\mathcal{X},p,q,k}^{(1)} \pm \varepsilon_{\mathcal{X},p,q,k}, \tag{20}$$

$$\hat{\gamma}_{\mathcal{X},p,q,k}^{(2)} = 1 - \hat{\gamma}_{\mathcal{X},p,q,k}^{(1)}, \tag{21}$$

where $\mathcal{X} \in \{\mathcal{A}, \mathcal{R}\}$, $p \in \{1, 2, \ldots, P'\}$, $q \in \{1, 2, \ldots, Q'\}$, $k \in \{1, 2, 3\}$ and $\varepsilon_{\mathcal{X},p,q,k}$ denotes the estimation error of $\hat{\gamma}_{\mathcal{X},p,q,k}^{(1)}$ at Eve. Additionally, the reference images that Eve estimates, corresponding to those used by Alice and the Relay, can be designated as $\hat{\mathbf{W}}_{\mathcal{A}}^{(ref)}$ and $\hat{\mathbf{W}}_{\mathcal{R}}^{(ref)}$, respectively. Eve utilizes the information from the first and second time slots in an attempt to reconstruct the original image. The process for this reconstruction follows specific steps outlined in the communication protocol.

$$\hat{\mathbf{W}}_{\mathcal{E}}^{(1)} = \left(\bar{\mathbf{W}}_{\mathcal{E}}^{(1)} - \hat{\mathbf{N}}_{\mathcal{A},2} \otimes \hat{\mathbf{W}}_{\mathcal{A}}^{(ref)}\right) \oslash \hat{\mathbf{N}}_{\mathcal{A},1}, \tag{22}$$

$$\hat{\mathbf{W}}_{\mathcal{E}}^{(2)} = \left(\bar{\mathbf{W}}_{\mathcal{E}}^{(2)} - \hat{\mathbf{N}}_{\mathcal{R},2} \otimes \hat{\mathbf{W}}_{\mathcal{R}}^{(ref)}\right) \oslash \hat{\mathbf{N}}_{\mathcal{R},1}. \tag{23}$$

Eve may then recover the whole size of the SR original image using VDSR ISR in the i-th time slot, where $i \in \{1, 2\}$, as

$$\hat{\mathbf{W}}_{\mathcal{E}}^{(SR,i)} = \Delta_{\tau}(\hat{\mathbf{W}}_{\mathcal{E}}^{(i)}). \tag{24}$$

As a result, at Eve the recovered image from both time slots are combined similarly at Bob.

$$\hat{\mathbf{W}}_{\mathcal{E}}^{(SR)} = \hat{\alpha}_1 \hat{\mathbf{W}}_{\mathcal{E}}^{(SR,1)} + \hat{\alpha}_2 \hat{\mathbf{W}}_{\mathcal{E}}^{(SR,2)}, \tag{25}$$

where $\hat{\alpha}_i$, $i \in \{1, 2\}$, represents the estimated Alpha blending fraction of the i-th SR image in the composite image at Eve.

For additional clarity, Fig.2 illustrates the workflow of the suggested SCR protocol for image transmission within a fading WRN. It confirms the existence of legitimate direct communication paths from Alice to Bob and relayed paths from Alice to Bob via the Relay. The diagram also indicates the potential for eavesdropping on both the direct Alice-to-Eve and the relayed Relay-to-Eve links.

5. Simulation Results

This section, the simulation outcomes of the suggested SCR method for secure image transmission over fading channels in WRNs are presented. The effectiveness of the proposed approach is evaluated using two performance metrics [40]: the Structural Similarity Index Measure (SSIM) and the Peak Signal-to-Noise Ratio (PSNR).

The PSNR is used to measure the quality of the image recovered by Bob, denoted as $\hat{\mathbf{W}}_{\mathcal{B}}^{(SR)}$, against the original superior-resolution (SR) image from Alice, $\mathbf{W}_{\mathcal{A}}^{(SR)}$. Meanwhile, the SSIM assesses the level of structural similarity between the recovered image $\hat{\mathbf{W}}_{\mathcal{B}}^{(SR)}$ and the original $\mathbf{W}_{\mathcal{A}}^{(SR)}$. Specifically, the PSNR [40] is calculated in decibels (dB) to quantify the image quality.

$$\begin{aligned}\text{PSNR} &\overset{(a)}{=} 10\log_{10}\frac{1}{\text{MSE}} \\ &\overset{(b)}{=} 10\log_{10}\frac{3PQ}{\sum_{x=1}^{P}\sum_{y=1}^{Q}\sum_{z=1}^{3}\left(\mathbf{W}_A(x,y,z) - \hat{\mathbf{W}}_B(x,y,z)\right)^2},\end{aligned} \tag{26}$$

In section (a), MSE represents the mean square error, which measures the discrepancy between the estimated superior-resolution image $\hat{\mathbf{W}}_{\mathcal{B}}^{(HR)}$ and the actual superior-resolution image $\mathbf{W}_{\mathcal{A}}^{(HR)}$. In section (b), it is acknowledged that RGB color images are typically considered to have dimensions $P \times Q$. Furthermore, by applying Eq.(26), one can calculate the PSNR for the image reconstructed by Eve through wiretap channels, which is a metric used to evaluate the quality of the reconstructed image.

The average SSIM of the restored picture at Bob, or $\hat{\mathbf{W}}_{\mathcal{B}}^{(HR)}$, is calculated using [49]:

$$\text{SSIM} = \frac{1}{PQ}\sum_{x=1}^{P}\sum_{y=1}^{Q}[b_{\mathcal{A},\mathcal{B}}(x,y)]^{\lambda}[c_{\mathcal{A},\mathcal{B}}(x,y)]^{\rho}[s_{\mathcal{A},\mathcal{B}}(x,y)]^{\theta}, \tag{27}$$

where the brightness, contrast, and structure components at pixel (x, y) are represented, respectively, by $b_{\mathcal{A},\mathcal{B}}(x,y)$, $c_{\mathcal{A},\mathcal{B}}(x,y)$, and $s_{\mathcal{A},\mathcal{B}}(x,y)$. In this case, λ, ρ, and θ denote the respective weighted combinations of these three elements.

In this simulation, MATLAB serves a dual purpose, being employed for both the training and validation phases. Training of the VDSR ISR network [24] is conducted using a dataset comprising 20,000 static, natural images from the IAPR TC-12 benchmark [47]. The VDSR ISR network is characterized by its architecture, which includes 20 convolutional layers, and processes 64 image patches, each measuring 41 by 41 pixels, with scaling factors ranging from 2 to

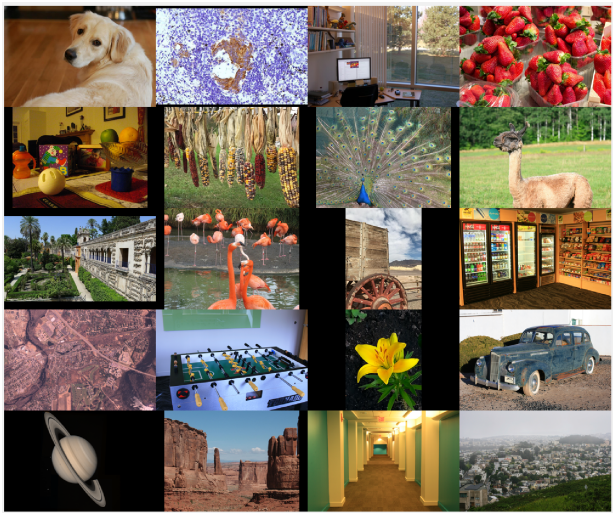

Figure 3. Images for testing and validation of the proposed cooperative secure image super-resolution.

10. Specifically, the network's initial layer contains 64 filters, each 3x3 in size, followed by 18 layers that alternate between convolutional operations and the application of the ReLU function. The second-to-last layer consists of a single convolutional filter, also 3x3x64, and the final layer employs a regression approach to determine the mean square error between the residual image and the network's prediction.

The training process utilizes specific hyperparameters: gradient clipping with an L2-norm technique and a threshold of 0.01, a momentum value of 0.9, and an initial learning rate of 0.1, which decreases tenfold every 10 epochs until reaching 100 epochs. For validation, 20 pristine images from MATLAB's Image Processing Toolbox, shown in Fig.3, are used.

Significantly, this study pioneers the integration of SCR with RLNC and VDSR ISR to enhance secure image communication over fading WRNs. The fading channel employed in the simulation adheres to the flat Rayleigh model, and the simulation itself is executed using BPSK modulation alongside convolutional coding, utilizing the generator pattern [111; 101].

5.1. SCR versus SRT versus SDT

Figure 4 illustrates the relationship between PSNR and SSIM values and the SNR (in dB) under Rayleigh fading conditions for the direct link between Alice and Bob (SDT) during the initial time slot, as well as the relay link through Relay (SRT) across both time slots, employing both the DF protocol and the suggested SCR protocol which is the simple image fusion technique where two images are overlayed and blended with Alpha blending factor [48] .

The Figure 4 is results of simulation with parameters listed in Table 1. This Figure shows that, the SRT

Table 1. Simulation Parameters

Parameter Description	Value
Original SR images	1-4 in Fig.3
Running	10 loops
Reference image at Alice	17 in Fig.3
Reference image at Relay	17 in Fig.3
Location of Alice	$(0, 0)$
Location of Bob	$(0, 3)$
Location of Relay	$(1.6, 1)$
Location of Eve	$(1.4, -1)$
Path loss factor	$\beta = 2$
Channels	AWGN and Rayleigh
Downscale factor	$\tau = 10$
RLNC coefficients	$[0.3, 0.5]$
Modulation	BPSK
Channel coding	1/2 Convolution code
Diversity receiving	MRC
Image denoised	DnCNN [28]
Image super-resolution	VDSR [24]

protocol is dominant over SDT protocol and SCR is a little better than SRT's performance with SNR below around 28dB (intersection of SRT and SDT which is depending on the location of Relay investigated in figure 10, the intersection divides evaluated SNR into two range: low range SNR - below 28dB and high range SNR - above 28dB). In high range SNR above 28dB, SCR protocol gives better results than SDT and SRT protocols about 0.2dB and 1dB respectively. The recovery of Eve is very poor compared to the SCR (below around 9 dB), which mean that Eve is hardly able to recover the image that Alice wants to send to Bob. The evaluation by using SSIM techniques is also get the similar results. However, in high range SNR, SCR is outperform to SDT and SDT. In Figure 4, we compare the effects of the Rayleigh fading channel and the AWGN channel, as explored in [12]. The performance of the SDT, SRT, and SCR protocols is similar over both channels in the small and large SNR regions. This is because, in the small SNR region, the noise is too high for Bob to recover the image, while in the large SNR region, the influence of fading noise is minimal. However, in the middle SNR region, the performance of the SDT, SRT, and SCR protocols over the AWGN channel is better than over the Rayleigh fading channel.

The Figure 5 shows simulation results where Alice and Relay use different reference images which are 17 and 15, respectively. Others parameters are the same as in Figure 4 (simulation parameters in Table 1). In this case the differences are only in SRT and SCR protocol where combining receiver techniques is used (in case of Relay use the same reference image as Alice) or not used (in case of Relay use the different reference image

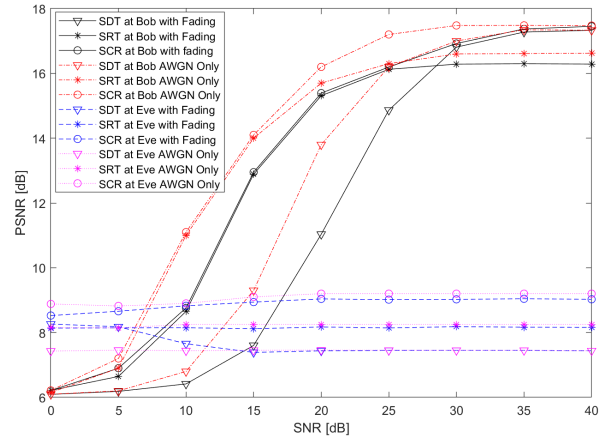

(a) PSNR vs SNR.

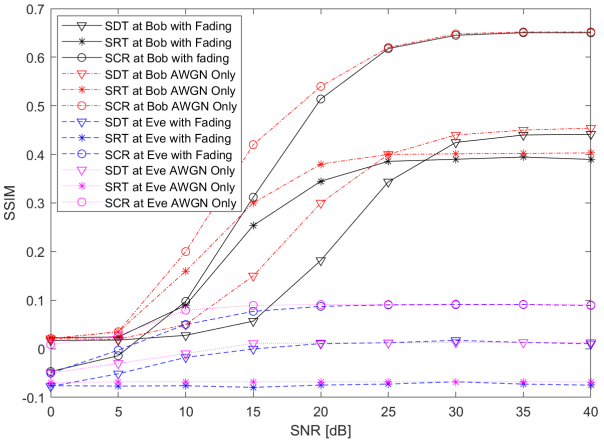

(b) SSIM vs SNR.

Figure 4. PSNR and SSIM of secure image communication protocols.

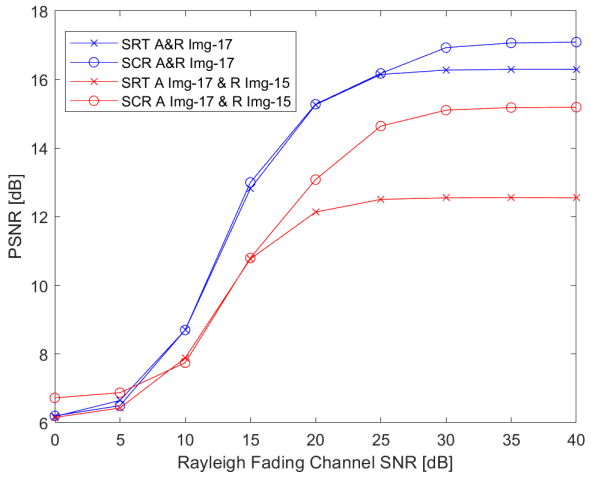

(a) PSNR vs SNR.

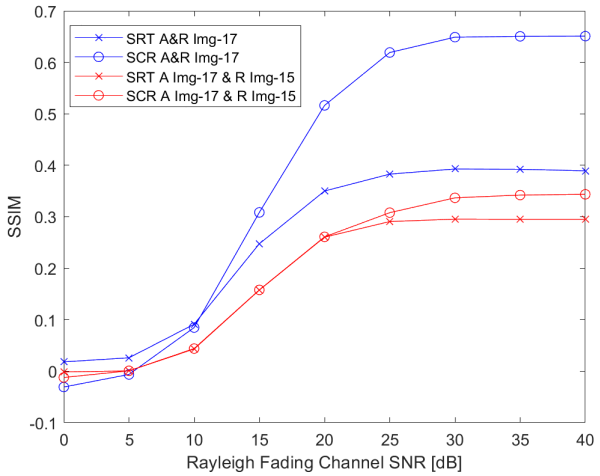

(b) SSIM vs SNR.

Figure 5. PSNR and SSIM of Relay use the same and different reference image from Alice.

as Alice). It shows that the performance of SCR and SRT which use diversity receiving are better then those protocol without using diversity receiving.

5.2. Effectiveness of diversity receiving for SCR

In this evaluation, we use the same simulation parameters as used in Figure 4 with different diversity receiving techniques such as MRC, EGC and SC. In Figure 6, it is show that, according to SNR value the performance of using MRC scheme is better from 0.2 to 0.4dB then those of using EGC and SC schemes in PSNR evaluation. In SSIM evaluation, the MRC technique is quite better than EGC and SC about 25% especially in high range SNR.

5.3. Impact of Scaling Factor

This section delves into the effects of varying the scale factor. Displayed in Figure 7 are the PSNR and SSIM metrics of the proposed SCR method in relation to the SNR with MRC receiving, considering different scaling factors, specifically $\tau = 2, 4, 6, 8, 10$. The simulation parameters remain consistent with those in Figure 4. At lower SNR levels, the PSNR and SSIM values across various scaling factors show minimal variance, largely due to the predominant influence of channel noise. Conversely, at higher SNR levels where channel noise diminishes, both PSNR and SSIM experience a decline, with PSNR dropping from 19dB to 17dB and SSIM from 0.74 to 0.63 as the scale factor increases from 2

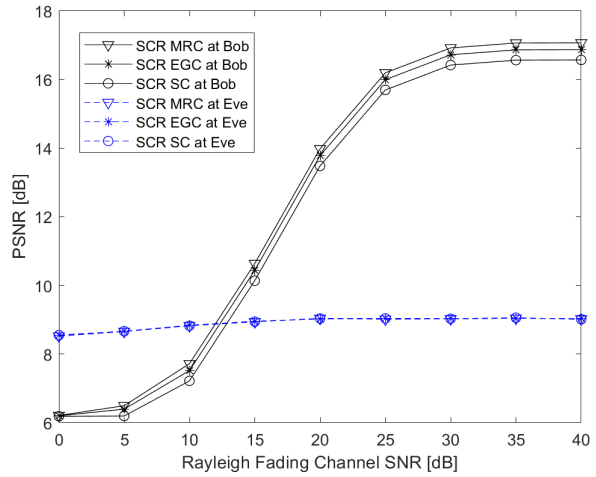

(a) PSNR vs SNR.

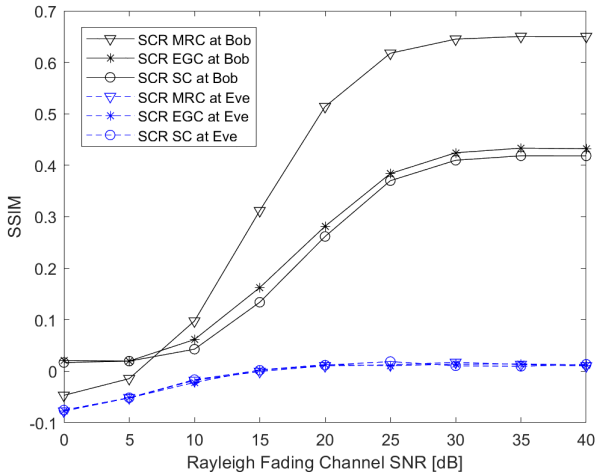

(b) SSIM vs SNR.

Figure 6. PSNR and SSIM of SCR with Diversity Receiving.

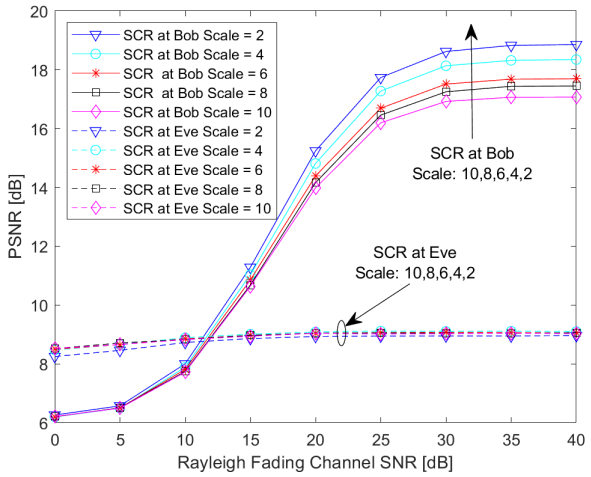

(a) PSNR vs SNR.

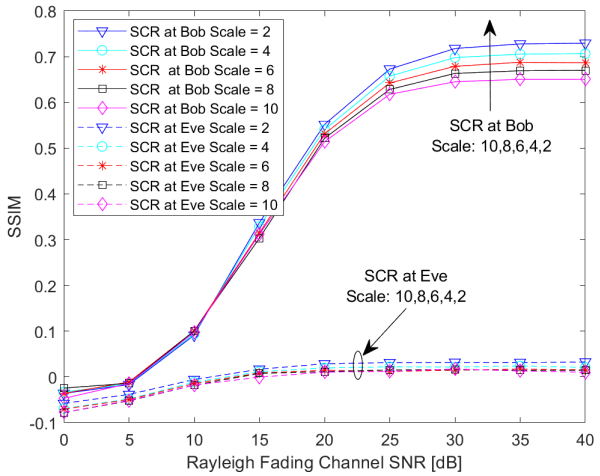

(b) SSIM vs SNR.

Figure 7. PSNR and SSIM of SCR with Different Scales.

to 10. Eve's ability to intercept the transmission is not markedly impacted by reducing the scale factor, since successful image decoding on Eve's part necessitates access to the RLNC coefficient matrices and the original images used by Alice and Relay for encoding, which are independent of the scale factor.

5.4. Impact of Reference and Estimation Image

Taking into account the impact of reference images, Figure 8 presents the PSNR and SSIM values against the SNR for various reference images utilized at Alice and Relay. Other simulation parameters are the same those used in Figure 4. Due to the different dimensions and structures of them, they impact too much to the proposed SCR protocol. The Figure 8 shows that in the low range SNR the impact of different reference images to SCR protocol are not too much for PSNR evaluation. However, they can differ too much in high range SNR i.e., PSNR of SCR with reference image number 17 can have around 4-4.3dB better performance then SCR with reference image number 15. The effect of reference images on PSNR and SSIM are not the same for example the PSNR's performance when working with image no 12 is better than its performance when working with image no 15, but SSIM's performance is in the opposite.

Figure 9 illustrates the effects of the wrong estimated images at Eve by plotting the PSNR and SSIM against SNR of the fading channel. The SCR protocol's performance is assessed with the same simulation conditions as those shown in Figure 4. When Eve

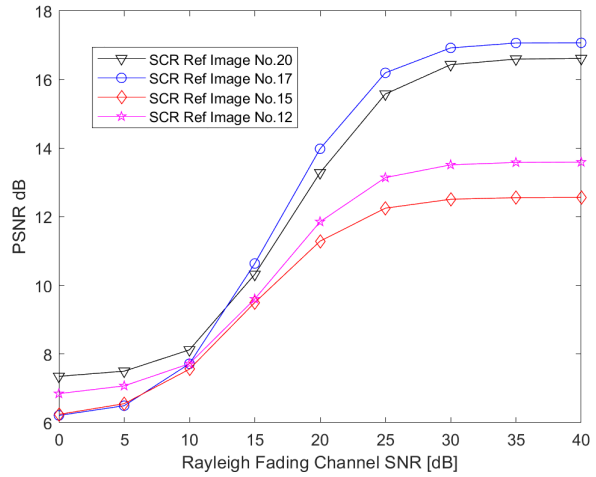

(a) PSNR vs SNR.

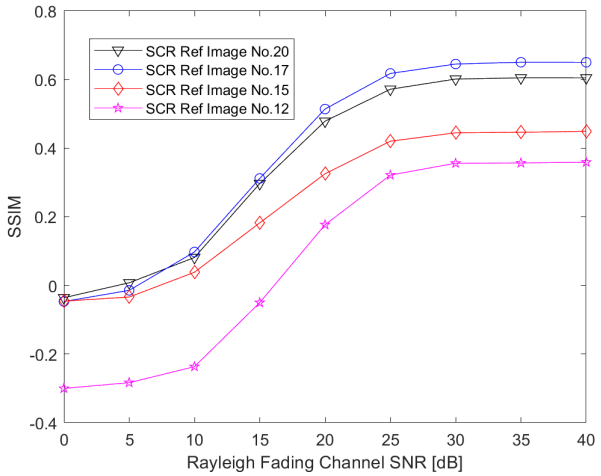

(b) SSIM vs SNR.

Figure 8. PSNR and SSIM of SCR with Different Reference Images.

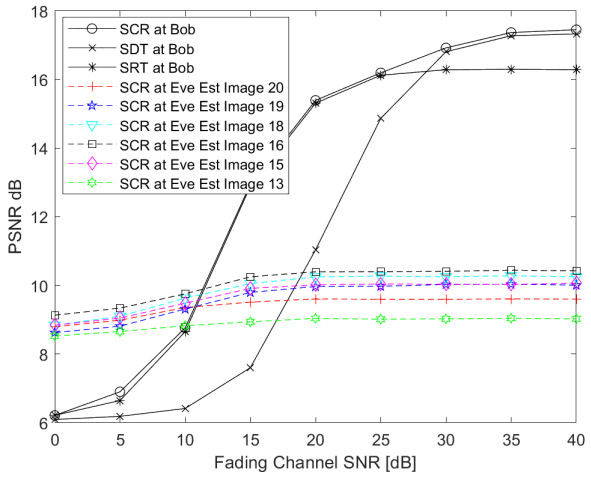

(a) PSNR vs SNR.

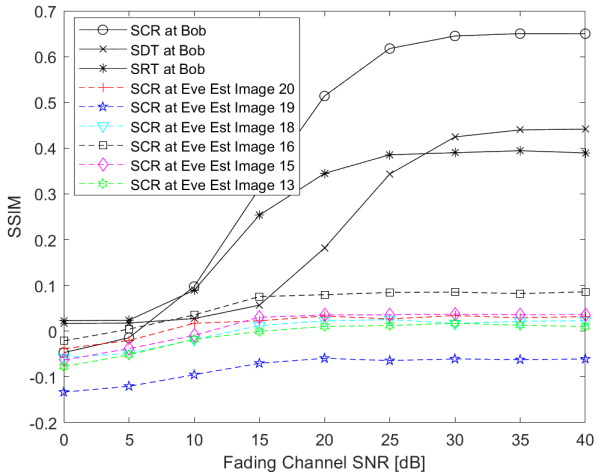

(b) SSIM vs SNR.

Figure 9. PSNR and SSIM of SCR at Eve with Different Estimated Images.

decodes the overheard images from Alice and Relay for the first and second time slots, respectively, utilizing a variety of wrong estimated photos, including the $13^{rd}, 15^{th}, 16^{th}, 18^{th}, 19^{th}$ and 20^{th} images (see Figure 3). Eve's performance is significantly harmed by the wrong estimated image, as shown in Figure 9. For example, Eve's best PSNR over fading channels using the 16^{th} estimated image is about 7.5dB less than Bob's, and Eve's performance is considerably worse when more incorrect estimated images are used for decoding. Different estimated images at Eve has different effect on Eve's performance. In general, wrong estimated image has poor recovering overheard image. Another fact that Eve is unaware of the RLNC coefficient matrices at Alice and Relay contributes to her poor performance as well. This demonstrates once more how successful the suggested SCR methodology is for safe picture transmission in WRNs.

5.5. The effect of Relay location

In order to evaluate the impact of Relay locations, we use the same simulation parameters as in Figure 4 and two more locations of Relay are taken into account such as $(1, 1)$ and $(2.2, 1)$. The Figure 10 shows that when changing locations of Relay the fading channel will effect to the $\mathcal{A} - \mathcal{R}$ and $\mathcal{R} - \mathcal{D}$ links only, Therefore, the performance of SDT are almost the same for all cases. The intersection of SRT and SDT divide fading channel into two ranges: low SNR range where SRT is dominant

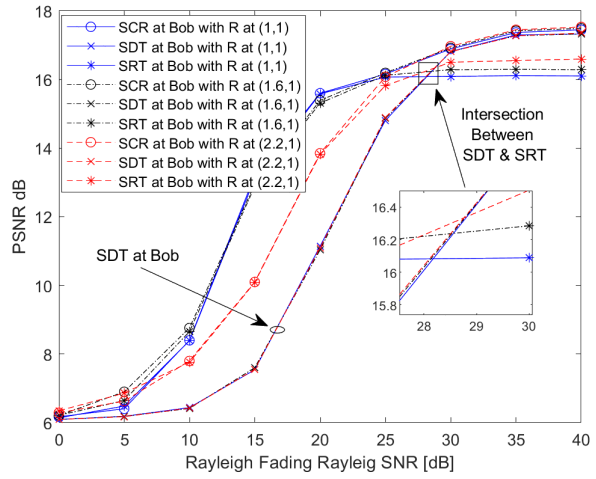

(a) PSNR vs SNR.

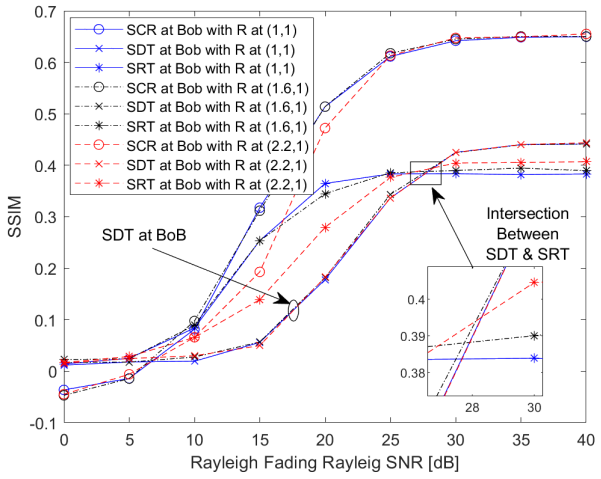

(b) SSIM vs SNR.

Figure 10. PSNR and SSIM of SCR at Bob with Different Relay Locations.

to SDT and high SNR range where SDT has better performance then SRT. In the low SNR range, the SCR is a little big better then SRT and SDT and the SCR of the Relay located near Bob has worse performance then those located near Alice and vice versa the SCR in case of the Relay located near Bob (i.e., Relay has location (2.2, 1)) has worse performance then those located near Alice (i.e., Relay has location (1, 1)).

6. Conclusion

For secure image communications in Rayleigh fading WRNs, where Alice wants to safely send SR photos to Bob via two hops with Relay's help, we have developed an SCR protocol in this study. At Alice and Relay, RLNC has been used to hide the original image from Eve. Additionally, VSDR ISR was used to recover the SR photos at Bob from their PR equivalents, which Alice had down-scaled before sending them to Bob and Relay. Research has demonstrated that, in comparison to Eve, the suggested SCR approach yields a significantly higher PSNR and SSIM at Bob of up to 7-7.5dB and 0.6-0.65 then those at Eve, respectively. The SCR protocol beats the SRT and SDT protocols by using direct and relaying links; in the low SNR range, SCR is slightly better than SRT and considerably better than SDT, whereas in the high SNR range, SCR is slightly better than SDT and much better than SRT. The positions of the relay determine the low and high SNR ranges. In addition to relying on relay locations, the proposed SCR protocol also depends on the reference image used. To increase SCR performance over the fading channel WRN, we can exploit the diversity receiver via relay and direct links such as MRC, EGC and SC receivers. Prior to being sent to Bob and Relay, the SCR protocol permits the original HR photos to be down-scaled to PR images up to 10 times in order to conserve transmission capacity. However, this results in a negligible reduction in image quality of less than 1 dB in the noisy environment (low SNR range) and around 2dB in high SNR range. Eve is specifically unable to decode the original SR photos due to her lack of knowledge of the RLNC coefficient matrices utilized at Alice and Relay as well as reference images in the common image datastore. Consequently, this validates and verifies the effectiveness of the suggested SCR technique in protecting the original SR image transmission in the Rayleigh fading WRNs with a constrained transmission bandwidth.

References

[1] A. Sendonaris, E. Erkip, and B. Aazhang, "User cooperation diversity. part i. system description," *IEEE transactions on communications*, vol. 51, no. 11, pp. 1927–1938, 2003.

[2] A. Nosratinia, T. E. Hunter, and A. Hedayat, "Cooperative communication in wireless networks," *IEEE communications Magazine*, vol. 42, no. 10, pp. 74–80, 2004.

[3] R. Ahlswede, N. Cai, S.-Y. Li, and R. W. Yeung, "Network information flow," *IEEE Transactions on information theory*, vol. 46, no. 4, pp. 1204–1216, 2000.

[4] R. H. Louie, Y. Li, and B. Vucetic, "Practical physical layer network coding for two-way relay channels: performance analysis and comparison," *IEEE Transactions on Wireless Communications*, vol. 9, no. 2, pp. 764–777, 2010.

[5] Q.-T. Vien, T. A. Le, H. X. Nguyen, and T. Le-Ngoc, "A physical layer network coding based modify-and-forward with opportunistic secure cooperative transmission protocol," *Mobile Networks and Applications*, vol. 24, pp. 464–479, 2019.

[6] T. Ho, M. Médard, R. Koetter, D. R. Karger, M. Effros, J. Shi, and B. Leong, "A random linear network coding approach to multicast," *IEEE Transactions on information theory*, vol. 52, no. 10, pp. 4413–4430, 2006.
[7] R. Koetter and M. Médard, "An algebraic approach to network coding," *IEEE/ACM transactions on networking*, vol. 11, no. 5, pp. 782–795, 2003.
[8] M. Ju and I.-M. Kim, "Error performance analysis of bpsk modulation in physical-layer network-coded bidirectional relay networks," *IEEE transactions on Communications*, vol. 58, no. 10, pp. 2770–2775, 2010.
[9] D. Nguyen, T. Tran, T. Nguyen, and B. Bose, "Wireless broadcast using network coding," *IEEE Transactions on Vehicular technology*, vol. 58, no. 2, pp. 914–925, 2008.
[10] E. Soljanin, "Lecture notes-network multicast with network coding," *IEEE Signal Processing Magazine*, vol. 25, no. 5, p. 109, 2008.
[11] L. Lima, M. Médard, and J. Barros, "Random linear network coding: A free cipher?" in *2007 IEEE International Symposium on Information Theory*. IEEE, 2007, pp. 546–550.
[12] H.-T. Duong, C. V. Phan, Q.-T. Vien, and T. T. Nguyen, "A secure cooperative transmission of image super-resolution in wireless relay networks," *Electronics*, vol. 12, no. 18, p. 3764, 2023.
[13] G. M. Davis and J. M. Danskin, "Joint source and channel coding for image transmission over lossy packet networks," in *Applications of Digital Image Processing XIX*, vol. 2847. SPIE, 1996, pp. 376–387.
[14] K. Stuhlmuller, N. Farber, M. Link, and B. Girod, "Analysis of video transmission over lossy channels," *IEEE Journal on selected areas in communications*, vol. 18, no. 6, pp. 1012–1032, 2000.
[15] Z. Zhang, Q. Sun, W.-C. Wong, J. Apostolopoulos, and S. Wee, "An optimized content-aware authentication scheme for streaming jpeg-2000 images over lossy networks," *IEEE Transactions on Multimedia*, vol. 9, no. 2, pp. 320–331, 2007.
[16] Z. Wang, J. Chen, and S. C. Hoi, "Deep learning for image super-resolution: A survey," *IEEE transactions on pattern analysis and machine intelligence*, vol. 43, no. 10, pp. 3365–3387, 2020.
[17] Y. K. Ooi and H. Ibrahim, "Deep learning algorithms for single image super-resolution: a systematic review," *Electronics*, vol. 10, no. 7, p. 867, 2021.
[18] W. Yang, X. Zhang, Y. Tian, W. Wang, J.-H. Xue, and Q. Liao, "Deep learning for single image super-resolution: A brief review," *IEEE Transactions on Multimedia*, vol. 21, no. 12, pp. 3106–3121, 2019.
[19] Z. Li, J. Yang, Z. Liu, X. Yang, G. Jeon, and W. Wu, "Feedback network for image super-resolution," in *Proceedings of the IEEE/CVF conference on computer vision and pattern recognition*, 2019, pp. 3867–3876.
[20] J.-H. Kim and J.-S. Lee, "Deep residual network with enhanced upscaling module for super-resolution," in *Proceedings of the IEEE conference on computer vision and pattern recognition workshops*, 2018, pp. 800–808.
[21] C. Dong, C. C. Loy, K. He, and X. Tang, "Learning a deep convolutional network for image super-resolution," in *Computer Vision–ECCV 2014: 13th European Conference, Zurich, Switzerland, September 6-12, 2014, Proceedings, Part IV 13*. Springer, 2014, pp. 184–199.
[22] W.-S. Lai, J.-B. Huang, N. Ahuja, and M.-H. Yang, "Deep laplacian pyramid networks for fast and accurate super-resolution," in *Proceedings of the IEEE conference on computer vision and pattern recognition*, 2017, pp. 624–632.
[23] S. G. Haris, Muhammad and N. Ukita, "Deep back-projection networks for super-resolution," in *Proceedings of the IEEE conference on computer vision and pattern recognition*, 2018, pp. 1664–1673.
[24] J. Kim, J. K. Lee, and K. M. Lee, "Accurate image super-resolution using very deep convolutional networks," in *Proceedings of the IEEE conference on computer vision and pattern recognition, Las Vegas, NV, USA*, 27-30 June 2016, pp. 1646–1654.
[25] J. Pan, N. Ye, H. Yu, T. Hong, S. Al-Rubaye, S. Mumtaz, A. Al-Dulaimi, and I. Chih-Lin, "Ai-driven blind signature classification for iot connectivity: A deep learning approach," *IEEE Transactions on Wireless Communications*, vol. 21, no. 8, pp. 6033–6047, 2022.
[26] Q.-T. Vien, T. Nguyen, and H. Nguyen, "A lightweight secure image super resolution using network coding," 2021.
[27] Y. Zhao, Y. Li, X. Dong, and B. Yang, "Low-frequency noise suppression method based on improved dncnn in desert seismic data," *IEEE Geoscience and Remote Sensing Letters*, vol. 16, no. 5, pp. 811–815, 2018.
[28] K. Zhang, W. Zuo, Y. Chen, D. Meng, and L. Zhang, "Beyond a gaussian denoiser: Residual learning of deep cnn for image denoising," *IEEE transactions on image processing*, vol. 26, no. 7, pp. 3142–3155, 2017.
[29] T. Rahim, S. Khan, M. A. Usman, and S. Y. Shin, "Exploiting de-noising convolutional neural networks (dncnns) for an efficient watermarking scheme: a case for information retrieval," *IETE Technical Review*, vol. 38, no. 2, pp. 245–255, 2021.
[30] D. M. Guerrini, Fabrizio and R. Leonardi, "Minimal information exchange for secure image hash-based geometric transformations estimation," *IEEE Transactions on Information Forensics and Security*, vol. 15, pp. 3482–3496, 2020.
[31] M. Kaur and V. Kumar, "A comprehensive review on image encryption techniques," *Archives of Computational Methods in Engineering*, vol. 27, no. 1, pp. 15–43, 2020.
[32] H. Peng, B. Yang, L. Li, and Y. Yang, "Secure and traceable image transmission scheme based on semitensor product compressed sensing in telemedicine system," *IEEE Internet of Things Journal*, vol. 7, no. 3, pp. 2432–2451, 2019.
[33] C.-K. Chan and L.-M. Cheng, "Hiding data in images by simple lsb substitution," *Pattern recognition*, vol. 37, no. 3, pp. 469–474, 2004.
[34] W. Bender, D. Gruhl, N. Morimoto, and A. Lu, "Techniques for data hiding," *IBM systems journal*, vol. 35, no. 3.4, pp. 313–336, 1996.
[35] E. Franz, A. Jerichow, S. Möller, A. Pfitzmann, and I. Stierand, "Computer based steganography: How it works and why therefore any restrictions on cryptography are nonsense, at best," in *Information Hiding: First International Workshop Cambridge, UK, May 30–June 1, 1996 Proceedings 1*. Springer, 1996, pp. 7–21.

[36] P.-Y. Po-Yueh, H.-J. Lin *et al.*, "A dwt based approach for image steganography," *International Journal of Applied Science and Engineering*, vol. 4, no. 3, pp. 275–290, 2006.

[37] A. I. Hashad, A. S. Madani, and A. E. M. A. Wahdan, "A robust steganography technique using discrete cosine transform insertion," in *2005 International Conference on Information and Communication Technology*. IEEE, 2005, pp. 255–264.

[38] J. Qin, Y. Luo, X. Xiang, Y. Tan, and H. Huang, "Coverless image steganography: a survey," *IEEE access*, vol. 7, pp. 171 372–171 394, 2019.

[39] K. Shankar and M. Elhoseny, *Secure image transmission in wireless sensor network (WSN) applications*. Springer, 2019.

[40] A. Hore and D. Ziou, "Image quality metrics: Psnr vs. ssim," in *2010 20th international conference on pattern recognition*. IEEE, 2010, pp. 2366–2369.

[41] S. Zhang, S. C. Liew, and P. P. Lam, "Hot topic: Physical-layer network coding," in *Proceedings of the 12th annual international conference on Mobile computing and networking*, 2006, pp. 358–365.

[42] Q.-T. Vien, H. X. Nguyen, B. G. Stewart, J. Choi, and W. Tu, "On the energy–delay tradeoff and relay positioning of wireless butterfly networks," *IEEE Transactions on Vehicular Technology*, vol. 64, no. 1, pp. 159–172, 2014.

[43] N. Cai and R. W. Yeung, "Secure network coding," in *Proceedings IEEE International Symposium on Information Theory,*. IEEE, 2002, p. 323.

[44] T. Cui, T. Ho, and J. Kliewer, "On secure network coding with nonuniform or restricted wiretap sets," *IEEE Transactions on Information Theory*, vol. 59, no. 1, pp. 166–176, 2012.

[45] A. S. Khan and I. Chatzigeorgiou, "Opportunistic relaying and random linear network coding for secure and reliable communication," *IEEE Transactions on Wireless Communications*, vol. 17, no. 1, pp. 223–234, 2017.

[46] S. E. Tajbakhsh, J. P. Coon, and G. Chen, "Network coding for physical layer secrecy," *IEEE Wireless Communications Letters*, vol. 7, no. 4, pp. 642–645, 2018.

[47] M. Grubinger, P. Clough, H. Müller, and T. Deselaers, "The iapr tc-12 benchmark: A new evaluation resource for visual information systems," in *International workshop ontoImage'2006 Language Resources for Content-Based Image Retrieval, held in conjunction with LREC'06, Genoa, Italy,*, vol. 2, pp 13-23, 22-May 2006.

[48] T. Porter and T. Duff, "Compositing digital images," in *Proceedings of the 11th annual conference on Computer graphics and interactive techniques*, 1984, pp. 253–259.

[49] Z. Wang, A. C. Bovik, H. R. Sheikh, and E. P. Simoncelli, "Image quality assessment: from error visibility to structural similarity," *IEEE transactions on image processing*, vol. 13, no. 4, pp. 600–612, 2004.